scientific reports

Check for updates

OPEN

# Repurposing of apoptotic inducer drugs against *Mycobacterium tuberculosis*

Kudakwashe Nyambo[1,2,3,8], Vivette Soko[1,2,3,8], Kudzanai Ian Tapfuma[1,2,3], Bongani Motaung[1,2,3], Francis Adu-Amankwaah[1,2,3], Lauren Julius[1,2,3], Ashwil Klein[4], Marshall Keyster[4], Lucinda Baatjies[1,2,3], Liezel Smith[1,2,3], Krishna Kuben Govender[6,7], Mkhuseli Ngxande[5], Andre G. Loxton[1,2,3]✉ & Vuyo Mavumengwana[1,2,3]✉

**Computational approaches complement traditional *in-vitro* or *in-vivo* assays, significantly accelerating the drug discovery process by increasing the probability of identifying promising lead compounds. In this study, the apoptotic compounds were assessed for antimycobacterial activity and immunomodulatory potential in infected THP-1 macrophage cells. The antimycobacterial activity of the apoptotic compounds was evaluated using the minimum inhibitory concentration (MIC) assay. The immunomodulatory potential of the apoptotic compounds was determined on mycobacterial-infected THP-1 and non-infected THP-1 macrophage cells. The potential binding dynamics of the compounds against InhA were predicted using molecular docking, molecular dynamics, and MM-GBSA binding free energies. The *in-vitro* MIC assay showed that cepharanthine (CEP) had the highest antimycobacterial activity against *Mycobacterium smegmatis* mc$^2$155 and *Mycobacterium tuberculosis* H37Rv, with MICs of 3.1 and 1.5 µg/mL, respectively, followed by CP-31398 dihydrochloride hydrate (DIH) (MICs = 6.2 and 3.1 µg/mL, respectively), marinopyrrole A (MAR) (MICs = 25 and 12.5 µg/mL, respectively), and nutlin-3a (NUT) (MICs = 50 and 25 µg/mL, respectively). MICs for the rest of the drugs were > 200 µg/mL against both *M. smegmatis* mc$^2$155 and *M. tuberculosis* H37Rv. Furthermore, the growth of *M. smegmatis* mc$^2$155 in infected THP-1 macrophage cells treated with DIH, CEP, carboxyatractyloside potassium salt (CAR), and NUT was inhibited by the mentioned drugs. Cytokine profiling showed that DIH optimally regulated the secretion of IL-1β and TNF-α which potentially enhanced the clearance of the intracellular pathogen. Molecular dynamics simulations showed that NUT, MAR, 17-(allylamino)-17-demethoxygeldanamycin (17-AAG), and BV02 strongly bind to InhA. However, 17-AAG and BV02 did not show significant activity *in-vitro*. This study highlights the importance of probing already existing chemical scaffolds as a starting point for discovery of therapeutic agents against *M. tuberculosis* H37Rv using both pathogen and host directed approaches. The integration of molecular dynamics simulations provides valuable insights into potential scaffold modifications to enhance the affinity.**

**Keywords** Drug repurposing, Tuberculosis, Host-directed therapy, Cytokine profiling, Molecular dynamics simulation

Tuberculosis (TB) is a severe and life-threatening infectious disease caused by a highly specialized human intracellular pathogen, *Mycobacterium tuberculosis*[1]. Standard chemotherapy and chemoprophylaxis treatment for drug-susceptible *M. tuberculosis* involves a six-month administration of a combination of first-line drugs, such as isoniazid (INH), ethambutol (ETH), rifampicin (RIF), and pyrazinamide (PZA), with a success rate

[1]DSI-NRF Centre of Excellence for Biomedical Tuberculosis Research, Stellenbosch University, Cape Town, South Africa. [2]South African Medical Research Council Centre for Tuberculosis Research, Stellenbosch University, Cape Town, South Africa. [3]Division of Molecular Biology and Human Genetics, Faculty of Medicine and Health Sciences, Stellenbosch University, Cape Town, South Africa. [4]Department of Biotechnology, University of Western Cape, Bellville, Cape Town, South Africa. [5]Computer Science Division, Department of Mathematical Sciences, Faculty of Science, University of Stellenbosch, Matieland, South Africa. [6]Department of Chemical Sciences, Doornfontein Campus, University of Johannesburg, P. O. Box 17011, Johannesburg 2028, South Africa. [7]National Institute for Theoretical and Computational Sciences (NITheCS), Stellenbosch, South Africa. [8]These authors contributed equally: Kudakwashe Nyambo and Vivette Soko. ✉email: gl2@sun.ac.za; vuyom@sun.ac.za

of 85%[2,3]. Isoniazid is a prodrug activated by the enzyme catalase-peroxidase (KatG), forming adducts with nicotinamide adenine dinucleotide (NAD). These adducts inhibit the activity of enoyl-ACP reductase (InhA), leading to *M. tuberculosis* death[4]. However, the emergence of drug-resistant strains, such as those with genetic mutations in genes like *KatG*, thaws the efforts of the global campaign to end TB. Moreover, *M. tuberculosis*'s metabolic adaptation to the host lung microenvironment contributes to the development of drug-resistant strains[5]. This highlights the urgent requirement for alternative strategies to address the rapid increase in drug-resistant TB.

The outcome of *M. tuberculosis* infection, whether the bacteria are drug-susceptible or drug-resistant, is determined by the ability of macrophages to modulate intracellular replication and the strategies employed by *M. tuberculosis* to avoid being killed by the macrophages[6,7]. Therefore, the progression of TB is influenced by the complex interaction between the macrophages and the *Mycobacterium* strain, both in terms of their phenotypic and genotypic features[8,9]. The production of cytokines and immune responses induced in both *in-vitro* and *in-vivo* models depends on the genotype and strain of *M. tuberculosis*. Therefore, it is essential to understand the gene expression of both the mycobacteria and host macrophages to comprehend the molecular mechanisms used by *M. tuberculosis* during an infection[9,10]. This knowledge is essential in developing strategies to combat TB disease. Repurposing apoptotic inducer drugs as potential *M. tuberculosis* agents may be an interesting approach to combat the pathogen and facilitate its clearance through apoptosis[11–13]. Previous research has shown that elesclomol, an apoptotic agent, exhibited a minimum inhibition concentration (MIC) of 4 mg/L against clinical isolates of extensively drug-resistant (XDR) *M. tuberculosis*[14]. Additionally, a combination of RIF and elesclomol effectively suppressed the intracellular growth of *M. tuberculosis* in bone marrow-derived macrophages. In another study, an anticancer drug with pro-apoptotic properties is also under investigation for its application as a host-directed therapeutic for treating TB[15].

In this study, 12 apoptotic inducer drugs from various classes were selected for repurposing as antitubercular agents. Minimum inhibition concentration (MIC) assays were conducted to determine the compounds whole-cell activity against *Mycobacterium smegmatis* $mc^2155$ and *M. tuberculosis* H37Rv. This was followed by a host-directed evaluation of compounds to stimulate clearance of *M. smegmatis* $mc^2155$ in infected THP-1 macrophage cells and the production of cytokines during treatment, which were measured using Luminex. The cell envelope of *M. tuberculosis* comprises mycolic acids and plays a critical role in the intricate immunomodulatory interaction between the bacterium and the host[16–18]. The biochemical pathways involved in the biosynthesis of mycolic acids comprise over 20 distinct multi-enzyme complexes that are well-characterized. One of the enzymes in the synthesis of mycolic acids is targeted by a prodrug called isoniazid. However, the increasing mutation rates of the *katG*, *kasA*, and *inhA* genes, which encode pro-drug activating enzymes, complicate TB treatment. Therefore, it is essential to develop new therapeutic agents that possess a specific mode of action and do not require prior activation[19]. Herein, the apoptotic inducer drugs were evaluated for potential strong binding dynamics to InhA using molecular docking, molecular dynamics simulations, and binding free energy calculations.

## Materials and methods

### Evaluation of antimycobacterial activity against M. smegmatis $mc^2155$ and M. tuberculosis H37Rv to determine MICs

Antimycobacterial inhibitory assays were performed to evaluate the bioactivity of the selected 12 apoptotic inducer drugs in Fig. 1, Table S1, and Table S2 (Sigma-Aldrich, Missouri, United States) against *M. smegmatis* $mc^2155$ and *M. tuberculosis* H37Rv.

The drugs were initially dissolved in dimethyl sulfoxide (DMSO) to make a stock solution of 10 mg/mL and stored at -20 °C. Working stocks were prepared by diluting with Middlebrook 7H9 broth (Becton, Dickinson and Company, New Jersey, United States), supplemented with 2% glycerol, 0.2% Tween-80 (v/v), and 10% Middlebrook oleic albumin dextrose catalase (OADC) (Becton, Dickinson and Company, New Jersey, United States).

Cultures of *M. smegmatis* $mc^2155$ and *M. tuberculosis* H37Rv were maintained as previously described Tapfuma et al.[20]. Inoculum for treatment was prepared using bacterial cultures at the exponential phase ($OD_{600}$ nm = 0.4–0.6). The addition of drugs and serial micro-dilution on 96-well plates was then performed to obtain a range of concentrations. After adding the inoculum to 96-well plates, the final volume in each well was 200 µL with the concentration of bacteria at a calculated $OD_{600}$ nm of 0.002–0.003. Treatments were incubated at 37 °C for 72 h for *M. smegmatis* $mc^2155$ and 144 h for *M. tuberculosis* H37Rv. INH was used as the positive control. The MICs were determined by adding 0.2 mg/mL of resazurin dye as the colorimetric growth indicator. The experiments were conducted in three technical and biological replicates and the highest concentration tested for all the 12 drugs was 200 µg/mL.

### Thawing and culturing of THP-1 macrophage cells

The THP-1 cells (TIB-202) were obtained from ATCC (https://www.atcc.org/). The THP-1 macrophage cells cryopreserved stock was thawed and washed to eliminate any dimethyl sulfoxide (DMSO) used for preservation. For the washing process, 1 mL of the stock was transferred to 5 mL pre-warmed RPMI 1640 with L-glutamine (Lonza, Sigma-Aldrich, Missouri, United States), supplemented with 10% fetal bovine serum (FBS) (Gibco, Thermo Fisher Scientific, Massachusetts, United States) (culture medium), followed by centrifugation at 180 × *g* for five minutes. The DMSO-free cells were then suspended in 5 mL of the culture medium and placed into a 25 $cm^2$ tissue culture flask (Greiner, Lasec, South Africa). Incubation was conducted at 37 °C in a humidified incubator (ESCO Vivid Air, South Africa) with 5% $CO_2$ for four days or until reaching 80% confluency. The culture was centrifuged at 180 × *g* and the pellet was resuspended and sub-cultured. An aliquot, 250 µL of the resuspended pellet of the THP-1 culture was transferred into 20 mL of fresh culture media in a 250 $cm^2$ tissue

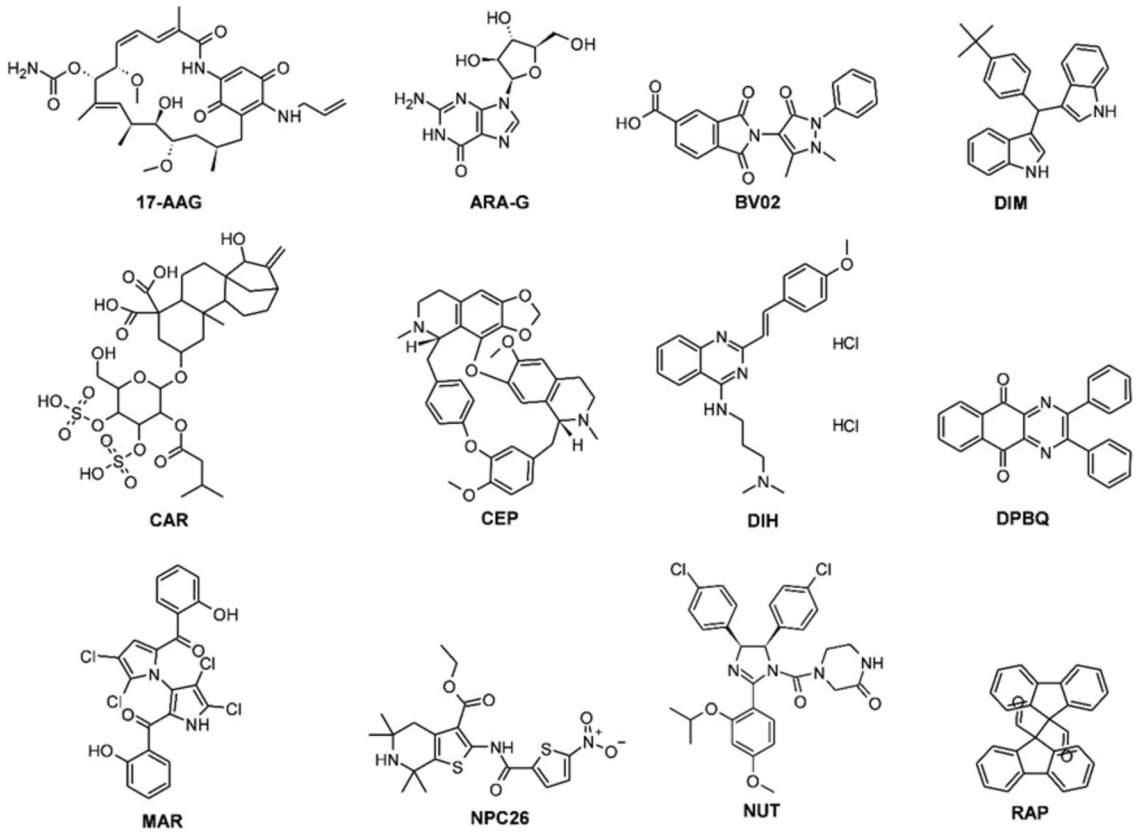


**Fig. 1**. Compound structures of the 12 apoptotic inducer drugs investigated in this study.

culture flask (Greiner, Lasec, South Africa), followed by incubation at 37 °C until the culture reached 80% confluence.

### Differentiation of THP-1 macrophage cells

The THP-1 cells from the confluent subculture were centrifuged and then suspended in fresh media. The cells were diluted to the desired density in culture media containing 50 µg/µL of phorbol 12-myristate 13-acetate (PMA) (Sigma-Aldrich, Missouri, United States) to differentiate the cells. Cells were seeded into either 96- or 24-well plates. The THP-1 macrophage cells were incubated for 72 h to facilitate their differentiation. After differentiation, the wells were washed twice with an equivalent volume of pre-warmed 1 × PBS, and the same volume of fresh media was added. Subsequently, the cells were incubated for 24 h to facilitate the recovery of THP-1 macrophages.

### Cytotoxicity analysis against THP-1 macrophage cells

Following the 24-h recovery phase, the cells were treated in triplicate with apoptotic inducer drugs at 25 µg/mL and then incubated for 24 h. A cytotoxicity assay was performed using 0.5 mg/mL of yellow tetrazolium salt (3-(4,5-dimethylthiazol-2-yl)-2,5-diphenyltetrazolium bromide or MTT), which was incubated for 4 h. The media was then carefully replaced with DMSO. The intensity of the purple formazan crystals was subsequently measured using a spectrophotometer, and the data were analysed using GraphPad Prism (Version 8.0.1 for Windows, GraphPad Software, San Diego, California, United States).

### In-vitro infection of THP-1 macrophage cell with M. smegmatis $mc^2155$

THP-1 macrophage cells were grown and differentiated as follows: The THP-1 macrophage cells were diluted to $2 \times 10^5$ cells/mL and one mL was dispensed per well of a 24-well plate. The non-pathogenic *M. smegmatis* $mc^2155$ was used as a surrogate for *M. tuberculosis* H37Rv. A cryopreserved *M. smegmatis* $mc^2155$ stock was cultured in 10 mL of 7H9 OADC (Difco, Becton, Dickinson and Company, New Jersey, United States) until reaching an $OD_{600}$ nm of 1.0. The bacterial culture was then washed twice through centrifugation at 4000 × *g* for 10 min in an equal volume of 1 × PBS. The pellets were resuspended in 5 mL of cell culture medium consisting of RPMI 1640 (Thermo Fisher Scientific, Massachusetts, United States) supplemented with 10% FBS. The resuspended cells were sonicated for 12 min at 37 °C to disrupt cell clumps. The bacterial cultures were filtered through a 40 µm filter, and the $OD_{600}$ nm was measured. To attain a desired Multiplicity of Infection (MOI) of approximately 2:1, a conversion factor of $OD_{600}$ nm of $1.0 = 1 \times 10^8$ bacteria was employed to dilute the bacterial cultures to obtain a MOI of 2:1. THP-1 cells were removed from the incubator, the spent medium was replaced with 1 mL of the freshly prepared culture, and media was added to the uninfected wells. The plates were then incubated at 37 °C in

a humidified incubator (ESCO Vivid Air, South Africa) with 5% $CO_2$ for three hours to facilitate the infection of THP-1 macrophage cells. Post-infection, the bacterial culture was removed, and THP-1 macrophage cells were treated with 1 mL of 1:100 penicillin (10,000 UI/mL, Sigma-Aldrich, Missouri, United States) diluted in RPMI medium. Plates were incubated at 37 °C for 40 to 60 min to allow the antibiotic to eliminate any extracellular bacteria. The wells were washed twice with 1 × PBS and treated with apoptotic inducer drugs for various time points.

Sampling was performed for each time point (0, 6, and 12). The supernatant was collected from representative wells for each treatment, then centrifuged and stored for cytokine analysis. The media was removed from all the wells, replaced with penicillin, and incubated for 40 to 60 min to eliminate any extracellular bacteria. The plates were again washed twice with 1 × PBS. Subsequently, 500 µL $dH_2O$ was added to the wells to lyse THP-1 macrophages. Each sample of lysed macrophage cultures (100 µL) was transferred to 900 µL of 1 × PBS containing 0.05% Tween-80, and serial dilutions were prepared up to $10^{-4}$. From these dilutions, 100 µL was plated in quarters on Middlebrook 7H10 agar and incubated at 37 °C to determine the CFU/mL. An uninfected control was plated, and no bacterial growth was expected on these plates. Colonies of mycobacteria were counted from two days onward for *M. smegmatis* $mc^2155$. The number of colonies was recorded as colonies forming units (CFU) and represented the number of intracellular mycobacteria that survived the apoptotic drug treatment.

## Cytokine analysis by Luminex technology

Samples intended for cytokine analysis were processed according to the manufacturer's instructions. A centrifugation speed of 4000 × *g* was chosen to precipitate the bacteria and macrophage debris, ensuring the retention of our proteins of interest in the supernatant. Cytokine production was measured using Luminex PROCARTAPLEX 13 PLEX (Thermo Fisher Scientific, Massachusetts, United States). The supernatants of THP-1 macrophage culture were collected during THP-1 infections with *M. smegmatis* $mc^2155$, as mentioned above. The samples collected at each point were *M. smegmatis* $mc^2155$ centrifuged at 4000 × *g* at 4 °C for 10 min to remove all bacteria and macrophage debris. The top layer of the supernatant was transferred into labelled tubes and stored at -80 °C until the day of cytokine analysis. Cytokines were quantified following the protocol as indicated by the manufacturer's instructions.

## Molecular docking

X-ray structure of InhA corresponding to PDB:6R9W with a resolution of 1.75 Å was retrieved from the protein data bank (https://www.rcsb.org/structure/). The protein preparation was performed as described by Nyambo et al.[21] in Schrödinger Release 2022–4. Hydrogen atoms were added, hydrogen-bond assignments were optimized, the loop was refined, and the OPLS4 (Optimized Potentials for Liquid Simulations 4) force field was used for energy minimization. The binding site was generated from the coordinates of the co-crystallized ligand (2 ~ {S})-1-(benzimidazol-1-yl)-3-(2,3-dihydro-1 ~ {H}-inden-5-yloxy)propan-2-ol using the Receptor Grid Generating module (Schrödinger Release 2022–4). The co-crystallized ligand (2 ~ {S})-1-(benzimidazol-1-yl)-3-(2,3-dihydro-1 ~ {H}-inden-5-yloxy)propan-2-ol, was used as the control. The apoptotic compounds were acquired from PubChem. (https://pubchem.ncbi.nlm.nih.gov/). The compounds were prepared using the LigPrep module (Schrödinger Release 2022–4) as previously described[22]. Briefly, the LigPrep energy minimized the compounds using the OPLS4 force field, generated ionization states at pH 7.0 ± 2.0 and generated multiple conformers per ligand. The control ligand was subjected to extra-precision (XP) molecular docking calculations against the selected target proteins using the Glide module (Schrödinger Release 2022–4)[23]. The root mean square deviation of the docked control ligand and undocked control ligand was calculated to verify the docking protocol. The apoptotic compounds were subjected to the verified XP docking protocol in the Glide module (Schrödinger Release 2022–4).

## Molecular dynamics simulations

The dynamic stability and molecular interactions of protein–ligand complexes generated from the XP docking were evaluated by performing 400 ns (ns) molecular dynamics (MD) simulations using Desmond (Schrödinger Release 2022–4). A total of seven MD systems were prepared in Maestro (Schrödinger Release 2022–4) as previously described[20]. Briefly, the TIP3P hydration model explicitly solvated the protein–ligand complex in an orthorhombic box with a buffer boundary dimension of (10 × 10 × 10 Å). The system was neutralized by adding counter ions ($Na^+$ and $Cl^-$) and sufficient NaCl was added to produce a 0.15 M buffer solution. For long electrostatic forces, periodic grid conditions were automatically generated for Particle-mesh Ewald Fast Fourier Transform (FFT). The entire system was energy-minimized and equilibrated at constant pressure (1.01325 bar) and temperature (303.15 K). The MD simulations were performed with the NPT ensemble. The Nose–Hoover thermostat was used with a 1.0 ps interval, and Martyna-Tobias-Klein was used as the default barostat with a 2.0 ps interval by applying an isotropic coupling style. The systems were subjected to MD simulations for 400 ns, and the internal energy was stored for every 1000 ps of the actual frame. The structural and dynamic behavior of the protein–ligand complexes were calculated by the Simulation Interaction Diagram module in Maestro (Schrödinger Release 2022–4) and represented as the root mean fluctuation (RMSF) and the root means square deviation (RMSD). The post-molecular dynamic simulation analysis was conducted by calculating the protein–ligand binding free energies based on MD simulation trajectories. The molecular mechanics generalised Born surface area (MM-GBSA) ($\Delta G_{bind}$) (kcal/mol) binding free energies were computed based on (Molecular Mechanics + Implicit Solvent Energy Function)[24].

## Statistical analysis

Statistical analyses were conducted using GraphPad Prism v.8.0.1. For infection data, multiple t-tests followed by the Holm-Sidak correction were performed to determine statistical significance with an α level of 0.05. Each

dataset was analyzed individually without assuming a consistent standard deviation, involving three separate t-tests. To address significant gaps between CFU values from technical and biological replicates, treatment efficacy was considered valid only if the ratio of post-treatment CFU to control CFU was 80% or higher, indicating 20% inhibition or less. Cytokine data were analyzed using ordinary two-way ANOVA in the same software.

## Results

### In-vitro antimicrobial activity against M. smegmatis mc$^2$155 and M. tuberculosis H37Rv

The antimycobacterial activity assays performed using the 12 repurposed apoptotic inducer drugs revealed that four, namely, CEP (1.5 µg/mL), DIH (3.1 µg/mL), NUT (12.5 µg/mL), and MAR (25 µg/mL) showed the highest antimycobacterial activity against *M. tuberculosis* H37Rv (Table 1). The rest of the drugs recorded MICs > 200 µg/mL against *M. smegmatis* mc$^2$155 and *M. tuberculosis* H37Rv.

### Cytotoxicity of the apoptotic inducer drugs against differentiated THP-1 macrophage cells

In the study, the cytotoxicity of apoptotic inducer drugs was evaluated against differentiated THP-1 macrophage cells, setting 80% cell viability as the minimum tolerable treatment concentration (Fig. 2). There was no significant difference between treated and untreated samples except for BV02, 17-AAG, MAR, and DIH treatments at 25 µg/mL.

### Growth inhibitory activity of selected apoptotic inducer drugs against M. smegmatis mc$^2$155 infected THP-1 cells

In this study, the efficacy of apoptotic inducer drugs against intracellular *M. smegmatis* mc$^2$155 was evaluated using the untreated THP-1 macrophage cells as the control sample. The drug MAR was excluded from subsequent assays due to limited resources and reports that nucleophiles can readily displace chlorides on pyrrole rings and also react with serum[25]. The results demonstrated that the investigated drugs, DIH, CEP, CAR, and NUT relatively inhibited the growth of intracellular *M. smegmatis* mc$^2$155 (Fig. 3). Particularly, CEP showed the maximum growth inhibition at 100% after 12 h of treatment at a concentration of 3.15 µg/mL (Fig. 3). A significant reduction in *M. smegmatis* mc$^2$155 relative survival was observed in DIH (6.25 µg/mL, $p = 0.0002$) and CEP (3.15 µg/mL, $p < 0.0001$) treated cells at 6 h post-treatment when compared to untreated samples. Furthermore, DIH (6.25 µg/mL), CAR (25 µg/mL), NUT (25 µg/mL), and CEP (3.15 µg/mL) significantly reduced *M. smegmatis* mc$^2$155 relative survival in THP-1 macrophages at 12 h post-treatment where $p < 0.0001$, $p = 0.0014$, $p = 0.0004$, and $p < 0.0001$, respectively.

### Cytokine analysis

This study determined the immunomodulatory potential of selected apoptotic inducer drugs using the cytokine expression profile. Cytokines expressed by macrophages in response to *M. smegmatis* mc$^2$155 infection were determined and are represented in Fig. 4. The heat-map analysis of evaluated apoptotic compounds revealed that these compounds are not immunogenic though the unaltered cytokine profiles in uninfected THP-1 macrophages at both 6- and 12-h post-exposure. The cytokine profile showed differential regulation by the apoptotic compounds where cytokines such as IFN-γ, IL-1β, IL-6, IL-13, IL-21, and IL-23 were reduced by the apoptotic compounds in uninfected THP-1 macrophages at both 6 h and 12 h. However, the secretion of IL-10, TNF-α, IL2, IL-5, and IL-22 showed differential upregulation by ARA-G, NPC26, and DIH in uninfected THP-1 macrophages at both time points. The apoptotic compounds were shown to enhance the secretion of cytokines in THP-1 macrophages following *M. smegmatis* mc$^2$155 infection at both 6 h and 12 h compared to untreated-infected samples.

| Drug | MICs (µg/mL) | |
|---|---|---|
| | *M. smegmatis* mc$^2$155 | *M. tuberculosis* H37Rv |
| 17-AAG | > 200 | > 200 |
| ARA-G | > 200 | > 200 |
| BV02 | > 200 | > 200 |
| CAR | > 200 | > 200 |
| CEP | 3.1 | 1.5 |
| DIH | 6.2 | 3.1 |
| DIM | > 200 | > 200 |
| DPBQ | > 200 | > 200 |
| MAR | 25–50 | 12.5 |
| NPC26 | > 200 | > 200 |
| NUT | 50 | 25 |
| RAP | > 200 | > 200 |
| INH | 32 | 16 |

**Table 1**. Antimycobacterial activity of apoptotic inducer drugs against *M. smegmatis* mc$^2$155 and *M. tuberculosis* H37Rv.

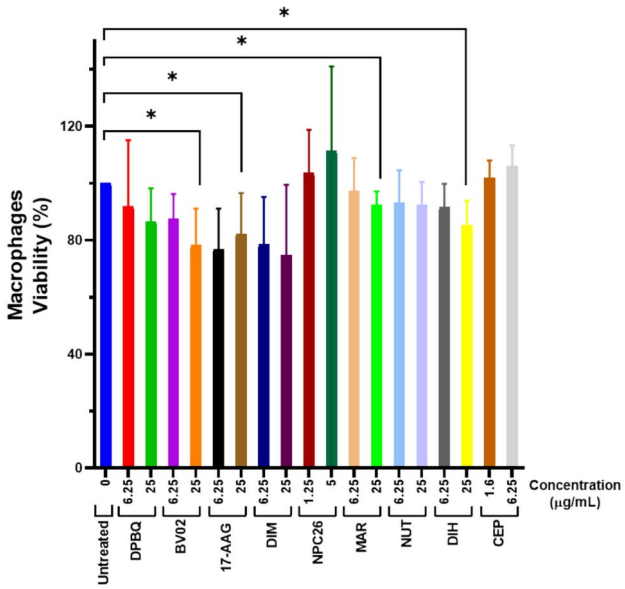


**Fig. 2**. Cytotoxicity profile of apoptotic inducer drugs against differentiated THP-1 macrophage cells. The healthy THP-1 macrophages were treated with various concentrations of the drugs corresponding to previously recorded MIC values against *M. smegmatis* mc$^2$155 and *M. tuberculosis* H37Rv. Data represents three technical and biological replicates where treated macrophages were analyzed against untreated controls. Data was interpreted as viable percentages and analyzed through ANOVA where $p \leq 0{,}05$*.

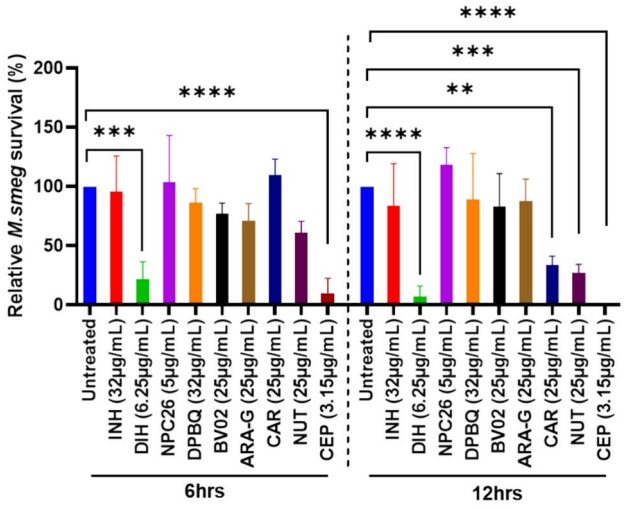


**Fig. 3**. Percentage survival of *M. smegmatis* mc$^2$155 (*M.smeg*) within THP-1 macrophages relative to untreated control at 6 and 12 h post-treatment with apoptotic inducer drugs. Data is a representative of three biological replicates and shown as mean ± SD. Two-way ANOVA followed by Dunnett's multiple comparison test was used for data analysis where significant difference is indicated as $p \leq 0.01$**, $p \leq 0.001$***, $p \leq 0.0001$****.

The results demonstrated that infected THP-1 macrophage cells showed an increased IL-1β secretion compared to uninfected THP-1 macrophages, with NPC26 and ARA-G constantly showing enhanced IL-1β secretion at both time points compared to the respective untreated samples post-infection (Fig. 5A). Apoptotic compounds did not stimulate TNF-α secretion in uninfected samples, except for ARA-G, which had elevated levels compared to untreated samples. However, this was reduced following infection at both time points. Contrary to ARA-G, all apoptotic compounds enhanced TNF-α secretion following the infection at both time points, where NCP26 and DIH-treated samples showed greater performance compared to untreated counterparts (Fig. 5B). On the other hand, IL-6 secretion was reduced by apoptotic compounds in uninfected THP-1 macrophages at 6 h post-treatment, whereas there were no changes observed at 12 h post-treatment when compared to untreated THP-1 macrophages. Following infection, IL-6 secretion showed an increase with INH and DPBQ at 6 h post-treatment with apoptotic compounds, while at 12 h an increase was only enhanced by DPBQ (Fig. 5C).

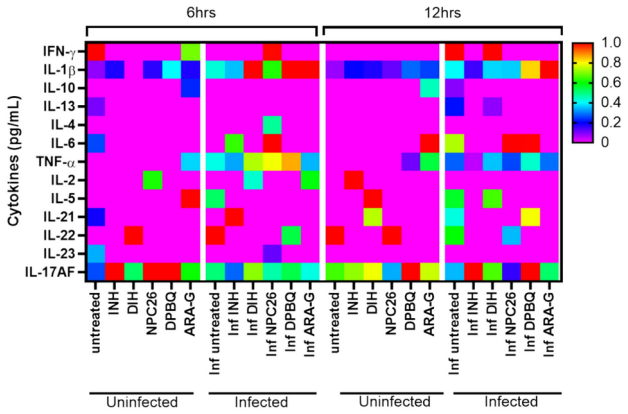


**Fig. 4**. Effect of apoptotic inducer drugs on the secretion of 13 selected cytokines in uninfected and *M. smegmatis* mc$^2$155-infected THP-1 macrophages. Cytokine expression was evaluated at two time points (6 and 12 h) in infected and uninfected THP-1 cells after treatment with apoptotic inducer drugs. Data was expressed in pg/mL and normalized per column where 0% (purple) was indicated by the lowest value and 100% (red) was indicated by the highest value.

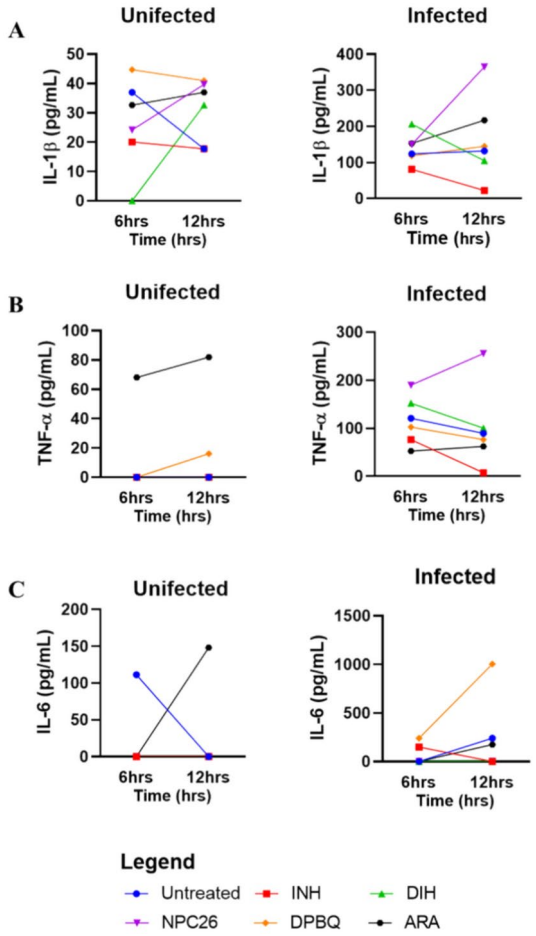


**Fig. 5**. Representative plots showing cytokine changes measured by Luminex multiplex assay in uninfected and *M. smegmatis* mc$^2$155 infected THP-1 macrophages (**A**): IL-1β, (**B**): TNF-α, (**C**): IL-6. Data were analyzed using two-way ANOVA.

## Molecular docking

The RMSD between the docked co-crystallized and original co-crystallized ligand was 1.93, thereby verifying the docking protocol (Figure S1). Notably, five apoptotic compounds have strong binding, ranging from an XP score of − 7.0 to − 9.3 kcal/mol (Table S3). The control ligand, (2 ~ {S})-1-(benzimidazol-1-yl)-3-(2,3-dihydro-1 ~ {H}-inden-5-yloxy)propan-2-ol, demonstrated an XP docking score of − 10.3 kcal/mol. Within the drugs, MAR demonstrated the strongest binding affinity (− 9.3 kcal/mol), followed by BV02 (− 8.6 kcal/mol), NUT (− 8.0 kcal/mol), 17-AAG (− 7.4 kcal/mol), and lastly, ARA-G (− 7.0 kcal/mol). MAR was found to interact with InhA residues through various bonds, as illustrated in Fig. 6A. Specifically, the ligand established a hydrogen bond between the Try158 amino acid residue of the protein and the carbonyl group of the ligand. The halogenated aromatic heterocyclic ring of the ligand also interacted through pi-pi stacking with Tyr158, while the ligand's aromatic hydrocarbon interacted with Lys165 through pi-cation. The ligand hydrophobically interacted with residues (Ile21, Ile95, Gly96, Met147, Phe149, Ala157, Thr158, Pro193, Ile194, Ala198, Met199, Ile202, Leu207, Ile215). The binding interaction between NUT and InhA residues involved forming five hydrogen bonds, as depicted in Fig. 6B. Specifically, the carboxamide group of NUT formed four hydrogen bonds with Gly14, Ile21, Ala22 and Ser94, while the imine group of the ligand formed a hydrogen bond with Thr196. The ligand also interacted with hydrophobic and polar residues in the binding pocket. BV02 interacts with InhA through two hydrogen bonds formed between Gly14 and Ser94, as shown in Fig. 6C. While 17-AAG formed one hydrogen bond with Thr196 as shown in Fig. 6D. Ara-G hydrate was deeply immersed in the hydrophobic binding pocket of InhA and interacted with Tyr158 through two pi-pi stacking interactions, as shown in Fig. 6E. Additionally, Asp148 formed a hydrogen bond with a hydroxyl group of ARA-G, while Ile194 also formed a hydrogen bond with a hydroxyl group of ARA-G.

MD simulations were used to evaluate the dynamics of the interactions between InhA and five apoptotic inducer drugs at a molecular level. The stability of the free protein was evaluated for 400 ns as a control as depicted in Figure S2. The stability of the InhA complexes was evaluated by computing RMSD and RMSF, while the drug affinity was determined using MM-GBSA. Specifically, NUT was strongly bound to InhA with an RMSD below 2.5 Å, as depicted in Fig. 7A. During the MD simulations, fluctuations were observed in InhA residues 100–110, but the rest of the system remained rigid, with RMSF values below 3 Å (Fig. 7B). During the 400 ns MD simulation, the InhA-NUT complex exhibited stability due to the formation of hydrogen bonds and water bridges with hydrophobic, polar, and positively charged amino acids (Fig. 7C). Gly14 formed a hydrogen bond with the drug's amide group for 33% of the simulation, Gly96 formed a hydrogen bond with the amide group for 34% of the simulation, and Thr196 formed a hydrogen bond with the heterocyclic nitrogen for 31% of the simulation. Ile31 formed a water bridge with the heterocyclic nitrogen of the drug for 31% of the simulation and Lys165 formed a water bridge with the carboxy group of the drug for 41% of the simulation.

During the 400 ns MD simulation period, the RMSD of InhA in complex with MAR exhibited a gradual increase from onset until reaching approximately 2 Å at around 50 ns and remaining stable until 350 ns. After that, it gradually increased to approximately 2.8 Å until 400 ns (Fig. 7D). This showed that the complex formed

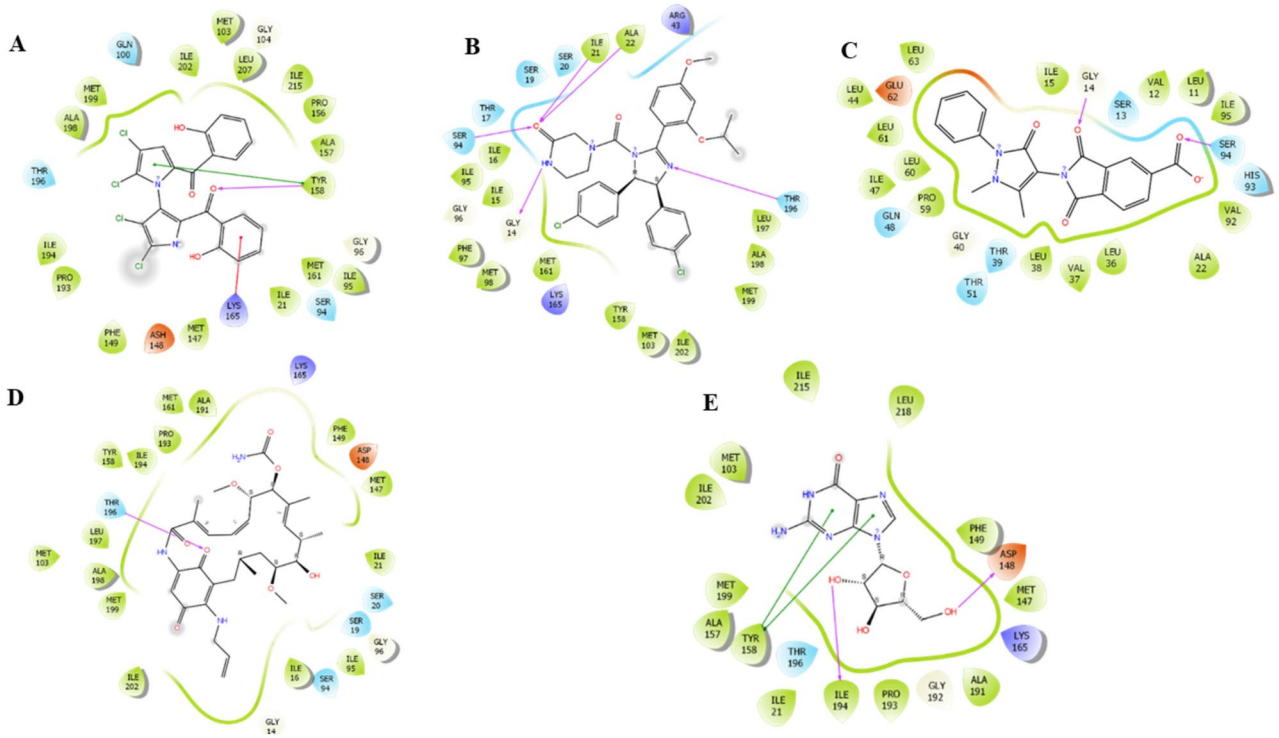


**Fig. 6**. Molecular interactions between InhA and (**A**) MAR (**B**) NUT (**C**) BV02 (**D**) 17-AAG (**E**) ARA-G.

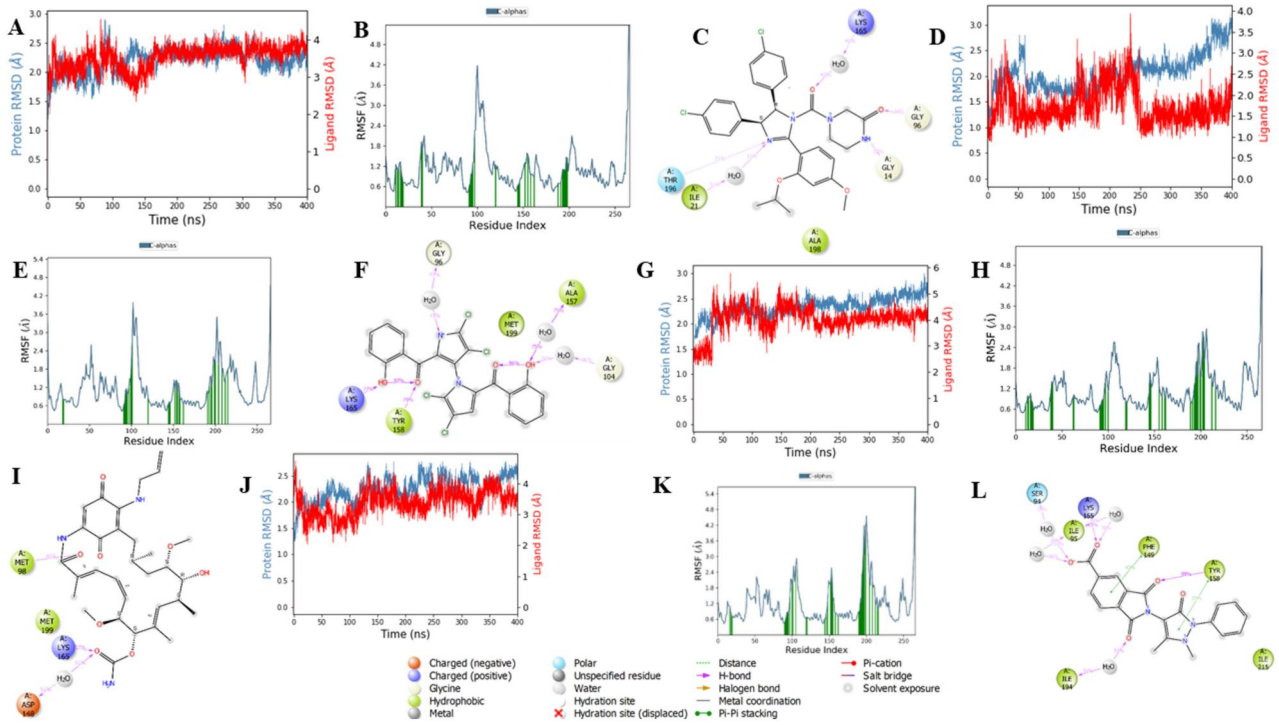


**Fig. 7**. Interaction dynamics of InhA upon binding of ligands. **(A)** RMSD of InhA Cα-atoms and NUT over a 400 ns simulation. **(B)** RMSF per residue of InhA in complex with NUT. **(C)** Interactions that occurred between InhA and NUT for more than 30% of the 400 ns MD simulation. **(D)** RMSD of InhA Cα-atoms and MAR over a 400 ns simulation. **(E)** RMSF per residue of InhA in complex with MAR. **(F)** Interactions that occurred between InhA and MAR for more than 30% of the 400 ns MD simulation. **(G)** RMSD of InhA Cα-atoms and 17-AAG over a 400 ns simulation. **(H)** RMSF per residue of InhA in complex with 17-AAG. **(I)** Interactions that occurred between InhA and 17-AAG for more than 30% of the 400 ns MD simulation. **(J)** RMSD of InhA Cα-atoms and BV02 over a 400 ns simulation. **(K)** RMSF per residue of InhA in complex with BV02. **(L)** Interactions that occurred between InhA and BV02 for more than 30% of the 400 ns MD simulation.

was stable. The drug, MAR, was very stable throughout the simulation period with an RMSD below 3 Å. The RMSD of the ligand's trajectory decreased from 2.5 Å to 1.5 Å between 200 and 250 ns. This decrease in RMSD could be attributed to the formation of two water bridges between Gly96 and the nitrogen of the halogenated cyclic heterocyclic ring at 250 ns as depicted in Figure S3A. The formation of the water bridge and halogen bond between ALA198 and the chloride atom of the ligand at 250 ns is illustrated in Figure S3B. Residues 100–110 were highly flexible during the simulation, as revealed by the RMSF analysis (Fig. 7E). Various interactions contributed to the stability of the complex interactions between InhA residues and MAR (Fig. 7F). These included hydrogen bonding between the hydrophobic Try158 and carbonyl group of MAR for 79% of the simulation duration, as well as between Lys165 and the hydroxyl group of MAR for 77% of the simulation duration. Water bridges were formed between Gly96 and the nitrogen of the halogenated cyclic heterocyclic ring for 47% of the simulation duration, between Gly104 and the hydroxyl group of the ligand, and between Ala157 and the hydroxyl group of MAR for 75% of the simulation duration. Furthermore, intramolecular hydrogen bonds were observed between the hydroxyl and carbonyl groups of MAR.

InhA bound to 17-AAG showed that the protein remained stable with an RMSD of approximately 2.4 Å (Fig. 7G). However, at 40 ns, there was a sudden increase in RMSD of 17-AAG, which then equilibrated at 4 Å for the rest of the simulation. The RMSF InhA residues analysis revealed that the system was rigid, with no residues fluctuating beyond 3 Å (Fig. 7H). During the 400 ns simulation, InhA and 17-AAG interacted through water bridges and hydrogen bonds (Fig. 7I). Specifically, a hydrogen bond between the hydrophobic Met98 and the amide group of the drug was observed for 40% of the simulation duration, while a hydrogen bond between the positively charged Lys165 and the amide group was present for 57% of the simulation duration. A water bridge was also formed between Asp148 and the amide group for 51% of the simulation duration.

The trajectory of InhA bound to BV02 remained stable at approximately 2.5 Å, while the RMSD of BV02 ranged at approximately 3.5 Å, as depicted in Fig. 7J. No significantly fluctuating InhA residues were observed in the RMSF analysis (Fig. 7K). The binding of BV02 to the active region of InhA was facilitated by various interactions, such as hydrogen bonds, water bridges, and pi-pi stacking, as illustrated in Fig. 7L. These interactions included a hydrogen bond between the hydrophobic Try158 and the carbonyl group, which lasted for 99% of the simulation. A hydrogen bond was also formed between the positively charged Lys165 and a carboxylic acid group for 36% of the simulation. Water bridges were observed between Ser94 and the carboxylic acid group of BV02 for 35% and between Ile95 and the carboxyl group of BV02 for 36% of the simulation. Additionally, pi-pi

| Complex | MM-GBSA $\Delta G_{bind}$ kcal/mol | $\Delta G_{bind}$ Coulomb kcal/mol | $\Delta G_{bind}$ Covalent kcal/mol | $\Delta G_{bind}$ Hbond kcal/mol | $\Delta G_{bind}$ *Solv GB* kcal/mol | $\Delta G_{bind}$ *Lipo* kcal/mol | $\Delta G_{bind}$ *vdW* kcal/mol |
|---|---|---|---|---|---|---|---|
| BV02 | − 78.9 | − 12.2 | 0.40 | − 1.50 | 22.2 | − 28.6 | − 55.8 |
| 17-AAG | − 65.7 | − 7.80 | 3.00 | − 0.80 | 24.1 | − 21.1 | − 62.3 |
| ARA-G | − 47.7 | − 22.9 | 3.30 | − 1.40 | 24.9 | − 12.0 | − 37.8 |
| NUT | − 79.9 | − 13.3 | 3.40 | − 0.70 | 24.6 | − 28.4 | − 65.3 |
| MAR | − 66.5 | − 61.7 | 2.50 | − 1.40 | 79.7 | − 26.3 | − 57.4 |
| Control Ligand | − 78.3 | − 22.1 | 1.80 | − 0.50 | 33.0 | − 30.9 | − 57.3 |

**Table 2**. MM-GBSA binding free energy computation. $\Delta G_{bind}$vdW = van der Waals contribution; $\Delta_{bind}$Covalent = covalent bonding contribution; $\Delta G_{bind}$Solv = polar contribution of solvation energy; $\Delta G_{bind}$Lipophilicity = lipophilicity energy contribution; $\Delta G_{bind}$Hbond = hydrogen bonding contribution; $\Delta G_{bind}$Coulomb = electrostatic interaction; $\Delta G_{bind}$ = binding free energy.

stacking was observed between Phe149 and the aromatic ring of BV02 for 43% of the simulation and between Tyr158 and the aromatic heterocyclic ring of BV02 for 35% of the simulation.

The RMSD of InhA bound to ARA-G gradually increased from the onset of the simulation and equilibrated at approximately 2.8 Å (Figure S4A). However, the RMSD of ARA-G gradually increased until 150 ns and equilibrated at 6 Å for the rest of the simulation. The RMSF revealed that only residues 105–110 fluctuated above 3 Å (Figure S4B). The interaction of InhA and the drug involved hydrogen bonds formed between Gly192 and the hydroxyl group of ARA-G, as well as between Ile194 and the hydroxyl group of ARA-G, as shown in Figure S4C.

The MM-GBSA was computed for the last 1500 frames. The binding free energy calculations showed varying affinity profiles exhibited by the apoptotic compounds towards the binding pocket of InhA as shown in Table 2. NUT exhibited the highest affinity towards InhA (− 79.9 kcal/mol), followed by BV02 (− 78.9 kcal/mol), while MAR had − 66.5 kcal/mol, followed by 17-AAG with an MM-GBSA free energy of − 65.7 kcal/mol. Lastly, ARA-G had the lowest affinity with an MM-GBSA free energy of (− 47.7 kcal/mol). A comparative analysis showed that NUT and BV02 exhibit a higher affinity towards the InhA binding site, in comparison to the control ligand.

## Discussion

The cell envelope of *Mycobacterium* plays a crucial role in the delicate immunomodulatory interplay between the bacterium and the host[26]. The envelope of *M. tuberculosis* consists of two distinct parts: the plasma membrane and the cell wall. The presence of mycolic acids in the cell wall core is of interest to drug discovery because it forms a hydrophobic permeability barrier, contributing to endogenous resistance of *M. tuberculosis* to many drugs[27,28].

Studies have revealed that remediation of the disease state is often achieved by killing the pathogen by inhibiting its molecular machinery used for cell wall biogenesis, sensing external signals, and inhibiting the formation of the phagolysosome [29,30]. The apoptotic inducer drugs were tested for their inhibitory efficacy against *M. smegmatis* $mc^2155$ and *M. tuberculosis* H37Rv. In this study, different classes of compounds namely, MAR, NUT, CEP, and DIH showed potent *in-vitro* activity against *M. smegmatis* $mc^2155$ and *M. tuberculosis* H37Rv. Furthermore, the cytotoxicity of apoptotic inducer drugs was determined on THP-1 macrophage cells to ensure the preliminary safety of the drugs. The results showed that the apoptotic inducer drugs used for treating THP-1 macrophages did not exhibit significant cytotoxicity. The *ex-vivo* inhibitory potential against *M. smegmatis* $mc^2155$ and immunomodulatory potential of the NPC26, DIH, CEP, and NUT were investigated. The findings of the study are in agreement with the research conducted by Jordao et al. and Sousa et al., which demonstrated the ability of THP-1 macrophage cells to exhibit a certain degree of inhibitory activity against the non-virulent *M. smegmatis* $mc^2155$[31,32]. Furthermore, the results showed that NPC26 did not facilitate intracellular elimination of *M. smegmatis* $mc^2155$. In contrast, DIH, CEP, and NUT were observed to enhance the clearance of intracellular *M. smegmatis* $mc^2155$, even at concentrations lower than the observed MICs. Treatment with NUT at 25 µg/mL inhibited 83% growth of intracellular bacteria after 12 h, which agrees with studies that demonstrated significant clearance of bacteria by NUT[32,33]. DIH or CEP at a concentration of 9.25 or 6.25 µg/mL, respectively, resulted in the total killing of intracellular bacteria within 6 h.

Early reports have indicated that the expression profile of cytokines by the host contributes to the severity of TB symptoms[34,35]. In this study, the infection of THP-1 macrophage cells with *M. smegmatis* $mc^2155$ resulted in the secretion of pro-inflammatory IL-1β and optimal concentrations of TNF-α, to combat the pathogen. Findings in this support a study by Roca et al. that reported that optimal concentrations of TNF-α enable the host to contain a pathogen infection[35]. Treatment of the infected THP-1 macrophage cells with DIH resulted in the secretion of pro-inflammatory IL-1β and optimal concentrations of TNF-α, which ultimately enhanced the elimination of intracellular *M. smegmatis* $mc^2155$. In contrast, excessive concentrations of TNF-α have been reported to increase trigger RIPK1- and RIPK3-dependent programmed necrosis, resulting in lyses of the infected macrophages as a result of increasing the extracellular bacteria burden[34,35].

To investigate the binding dynamics of the formed complexes, XP molecular docking, molecular dynamics simulations, and MM-GBSA binding free energies were computed. Among the drugs, NUT and BV02 showed the highest affinity towards the binding pocket of InhA. MAR and 17-AAG also exhibited a high affinity towards

InhA but slightly lower than that of NUT and BV02. ARA-G showed the lowest affinity towards InhA. The integration of targeted virtual screening could accelerate the identification of potential inhibitors and inform on potential modification on the chemical scaffolds to enhance the affinity to the target protein.

## Limitations

In our study, the 7H9 broth microdilution method was used for the preliminary drug susceptibility testing. However, the 7H9 broth microdilution method is less sensitive compared to BACTEC MGIT 960 method especially for isoniazid.

## Conclusion

*In-vitro* assays further showed that CEP, DIH, NUT, and MAR exhibited antimycobacterial activity. Interestingly, CEP and DIH exhibited low antimycobacterial activity 1.5 µg/mL and 3.1 µg/mL, respectively. Furthermore, three drugs, namely DIH, CEP, and NUT, were found to facilitate the clearance of *M. smegmatis* $mc^2155$ in THP-1 macrophage cells at concentrations lower than their respective MICs. Of these, DIH has been found to enhance the clearance of intracellular *M. smegmatis* $mc^2155$ by modulating the optimal secretion of IL-1β and TNF-α. Virtual screening strategies are highly effective in reducing both time and costs during drug discovery. The results of the simulations and MMGBSA binding free energy computation revealed that NUT, BV02, MAR, and 17-AAG have a high affinity towards InhA, with NUT exhibiting the strongest binding energy (–79.9 kcal/mol). The binding dynamics also provide valuable insights into regions where the compounds can be modified in relation to the three-dimensional space of active site of InhA.

## Data availability

The datasets generated during and/or analysed during the current study are available from the corresponding author upon request.

Received: 23 August 2024; Accepted: 18 February 2025
Published online: 28 February 2025

## References

1. Who. WHO consolidated guidelines on tuberculosis: tuberculosis preventive treatment. (2020).
2. Penn-Nicholson, A. et al. Detection of isoniazid, fluoroquinolone, ethionamide, amikacin, kanamycin, and capreomycin resistance by the Xpert MTB/XDR assay: A cross-sectional multicentre diagnostic accuracy study. *Lancet Infect. Dis.* **22**, 242–249 (2022).
3. Ge, F. et al. In vitro synergistic interactions of oleanolic acid in combination with isoniazid, rifampicin or ethambutol against Mycobacterium tuberculosis. *J Med. Microbiol.* https://doi.org/10.1099/jmm.0.014837-0 (2010).
4. Khalifa, A., Khalil, A., Abdel-Aziz, M. M., Albohy, A. & Mohamady, S. Isatin-pyrimidine hybrid derivatives as enoyl acyl carrier protein reductase (InhA) inhibitors against Mycobacterium tuberculosis. *Bioorg. Chem.* **138**, 106591 (2023).
5. Salina, E. G. & Makarov, V. Mycobacterium tuberculosis dormancy: How to fight a hidden danger. *Microorganisms* **10**, 2334 (2022).
6. Joosten, S. A., Fletcher, H. A. & Ottenhoff, T. H. M. A helicopter perspective on TB biomarkers: Pathway and process based analysis of gene expression data provides new insight into TB pathogenesis. *PLoS One* **8**, 73230 (2013).
7. Estrella, J. et al. A novel in vitro human macrophage model to study the persistence of mycobacterium tuberculosis using vitamin D3 and retinoic acid activated THP-1 macrophages. *Front .Microbiol.* https://doi.org/10.3389/fmicb.2011.00067 (2011).
8. Madhvi, A., Mishra, H., Leisching, G. R., Mahlobo, P. Z. & Baker, B. Comparison of human monocyte derived macrophages and THP1-like macrophages as in vitro models for M. tuberculosis infection. *Comp. Immunol. Microbiol. Infect. Dis.* **67**, 101355 (2019).
9. Feng, Z. et al. Differential responses by human macrophages to infection with mycobacterium tuberculosis and non-tuberculous mycobacteria. *Front. Microbiol.* https://doi.org/10.3389/fmicb.2020.00116 (2020).
10. Sharma, S., Sharma, M. & Bose, M. Mycobacterium tuberculosis infection of human monocyte-derived macrophages leads to apoptosis of T cells. *Immunol. Cell Biol.* **87**, 226–234 (2009).
11. Velmurugan, K. et al. Mycobacterium tuberculosis nuoG Is a virulence gene that inhibits apoptosis of infected host cells. *PLoS Pathog* **3**, 0972–0980 (2007).
12. Meena, L. S. & Rajni, T. Survival mechanisms of pathogenic Mycobacterium tuberculosis H37Rv. *FEBS J* **277**, 2416–2427 (2010).
13. Sly, L. M., Hingley-Wilson, S. M., Reiner, N. E. & McMaster, W. R. Survival of Mycobacterium tuberculosis in Host Macrophages Involves Resistance to Apoptosis Dependent upon Induction of Antiapoptotic Bcl-2 Family Member Mcl-1. *J. Immunol.* **170**, 430–437 (2003).
14. Ngwane, A. H. et al. The evaluation of the anti-cancer drug elesclomol that forms a redox-active copper chelate as a potential anti-tubercular drug. *IUBMB Life* **71**, 532–538 (2019).
15. Cleverley, T. L. et al. The host-directed therapeutic imatinib mesylate accelerates immune responses to Mycobacterium marinum infection and limits pathology associated with granulomas. *PLoS Pathog.* **19**, e1011387 (2023).
16. Xu, J. et al. A novel protein kinase inhibitor IMB-YH-8 with anti-tuberculosis activity. *Sci. Rep.* **7**(1), 1–10 (2017).
17. Singh, S., Singh, D., Hameed, S. & Fatima, Z. An overview of mycolic acids: structure–function–classification, biosynthesis, and beyond. In *Biology of Mycobacterial Lipids* 1–25 (Elsevier, 2022). https://doi.org/10.1016/B978-0-323-91948-7.00016-6.
18. Gavalda, S. et al. The Pks13/FadD32 crosstalk for the biosynthesis of mycolic acids in Mycobacterium tuberculosis. *J. Biol. Chem.* **284**, 19255–19264 (2009).
19. Zhang, Q., Han, J., Zhu, Y., Tan, S. & Liu, H. Binding thermodynamics and dissociation kinetics analysis uncover the key structural motifs of phenoxyphenol derivatives as the direct inha inhibitors and the hotspot residues of InhA. *Int. J. Mol. Sci.* **23**, 10102 (2022).
20. Tapfuma, K. I. et al. Antimycobacterial activity and molecular docking of methanolic extracts and compounds of marine fungi from Saldanha and False Bays. *S. Afr. Heliyon* **8**, e12406 (2022).
21. Nyambo, K. et al. Molecular docking, molecular dynamics simulations and binding free energy studies of interactions between Mycobacterium tuberculosis Pks13, PknG and bioactive constituents of extremophilic bacteria. *Sci. Rep.* **14**(1), 1–22 (2024).
22. Schrödinger. LigPrep | Schrödinger. *Schrödinger Release 2018–1* Preprint at (2021).
23. Friesner, R. A. et al. Glide: A new approach for rapid, accurate docking and scoring. 1. Method and assessment of docking accuracy. *J. Med. Chem.* **47**, 1739–1749 (2004).
24. Ejalonibu, M. A., Elrashedy, A. A., Lawal, M. M., Mhlongo, N. N. & Kumalo, H. M. Pharmacophore mapping of the crucial mediators of dual inhibitor activity of PanK and PyrG in tuberculosis disease. *Mol. Simul.* https://doi.org/10.1080/08927022.2021.2019251 (2022).

25. Fenical, W. Marine microbial natural products: the evolution of a new field of science. *J. Antibiot.* **73**(8), 481–487 (2020).
26. Xu, X. et al. Anti-tuberculosis drug development via targeting the cell envelope of Mycobacterium tuberculosis. *Front. Microbiol.* **13**, 1056608 (2022).
27. Kuang, W., Zhang, H., Wang, X. & Yang, P. Overcoming Mycobacterium tuberculosis through small molecule inhibitors to break down cell wall synthesis. *Acta Pharm. Sin. B* **12**, 3201–3214 (2022).
28. Savintseva, L. A. et al. Conformational dynamics and stability of bilayers formed by mycolic acids from the mycobacterium tuberculosis outer membrane. *Molecules* **28**, 1347 (2023).
29. Phusi, N. et al. Structure-based drug design of novel M. tuberculosis InhA inhibitors based on fragment molecular orbital calculations. *Comput. Biol. Med.* **152**, 106434 (2023).
30. Zeng, J. et al. Protein kinases PknA and PknB independently and coordinately regulate essential Mycobacterium tuberculosis physiologies and antimicrobial susceptibility. *PLoS Pathog* https://doi.org/10.1371/journal.ppat.1008452 (2020).
31. Jordao, L., Bleck, C. K. E., Mayorga, L., Griffiths, G. & Anes, E. On the killing of mycobacteria by macrophages. *Cell Microbiol.* **10**, 529–548 (2008).
32. Sousa, S., Borges, V., Joao, I., Gomes, J. P. & Jordao, L. Nontuberculous mycobacteria persistence in a cell model mimicking alveolar macrophages. *Microorganisms* **7**, 113 (2019).
33. Nuti, E. et al. Identification of a novel p53 modulator endowed with antitumoural and antibacterial activity through a scaffold repurposing approach. *Pharmaceuticals* **15**, 1318 (2022).
34. Roca, F. J. & Ramakrishnan, L. TNF dually mediates resistance and susceptibility to mycobacteria via mitochondrial reactive oxygen species. *Cell* **153**, 521–534 (2013).
35. Roca, F. J., Whitworth, L. J., Redmond, S. & Jones, A. A. TNF induces pathogenic programmed macrophage necrosis in tuberculosis through a mitochondrial-lysosomal-endoplasmic reticulum circuit. *Cell* **178**, 1344-1361.e11 (2019).


## Acknowledgements

Acknowledgments: We acknowledge the Open Access Fund of Stellenbosch University. We would also like to extend our appreciation to the Center for High-Performance Computing, South Africa, for providing us with access to the infrastructure used to conduct the simulations.We would also like to extend our appreciation to the Center for High-Performance Computing, South Africa, for providing us with access to the infrastructure used to conduct the simulations.

## Author contributions

Conceptualization, V.M., K.N., K.I.T., L.B., B.M., M.N., A.G.L., L.S.; methodology, V.M., K.N., V.S., A.G.L., K.I.T., K.K.G., and M.N; formal analysis, K.N., V.S. K.I.T and B.M; investigation, K.N., V.S.; resources, V.M., A.G.L., M.N., L.S., K.K.G., and L.B.; writing original draft preparation, K.N., V.S.; writing review and editing, V.M., M.N., A.G.L., K.K.G., K.I.T., L.B., L.S., B.M., L.J., A.K., M.K and FA.; supervision, V.M., A.G.L., M.N., K.K.G., L.S, and L.B; project administration, V.M., L.S., A.G.L., funding acquisition, V.M., A.G.L and L.S; Molecular docking and Molecular dynamics simulations, K.N., K.K.G., K.I.T., and M.N. All authors have read and agreed to the published version of the manuscript.

## Funding

This work was supported by the South African Medical Research Association Council (SAMRC), the Centre of Excellence for Biomedical Tuberculosis Research (CBTBR), and the National Research Fund (NRF) [NRF GRANT UID129364], National Research Fund (NRF) [Postdoctoral GRANT PSTD23041794183].

## Declarations

## Competing interests

The authors declare no competing interests.

## Ethical approval

Ethical approval for this study was approved by the Research Ethics Committee: Biological and Environmental Safety (REC: BES) of Stellenbosch University with reference number **BEE-2022–3188**.

## Additional information

**Supplementary Information** The online version contains supplementary material available at https://doi.org/10.1038/s41598-025-91096-8.

**Correspondence** and requests for materials should be addressed to A.G.L. or V.M.